Parameter Uncertainty Quantification applied to the Duisburg Propeller Test Case

Eduardo T. Katsuno[*‡], Artur K. Lidtke[*], Bülent Düz[*], Douwe Rijpkema[*] and Guilherme Vaz[*†§]
[*]MARIN - Maritime Research Institute Netherlands, [‡] USP - University of São Paulo, Brazil, [†]WavEC - Offshore Renewables, Portugal, [§] ISMT, University of Duisburg-Essen, Duisburg/Germany
eduardo.katsuno@usp.br

1 Introduction

At model-scale conditions (diameter-based Reynolds number below 10^6), laminar-to-turbulent transition plays an important role on the performance of a propeller. While at these Reynolds numbers turbulent transition and its effects on the flow are difficult to simulate, current state-of-the-art transition models (Menter et al. (2004)) provide viable means to do so. Previous studies on these new methods (Eça et al. (2016), Baltazar et al. (2018), Lopes et al. (2018)) show that, as in reality, the results are sensitive to the inlet turbulence intensity and its decay upstream of the propeller plane. In the aforementioned studies, numerical uncertainties were reported to have been small. Therefore, it is expected that variability of the user-specified inflow conditions will have a dominant effect on the solution.

To better understand the associated uncertainty of model-scale open-water propeller performance predictions, Uncertainty Quantification (UQ) methods are employed in this work. Given a prescribed range of input uncertainties reflecting typical ranges found in test facilities and RANS simulation setups, a laminar-turbulent transition model is used in CFD simulations of the Duisburg Propeller Test Case. This paper then aims to use the results in order to quantify the parameter uncertainty and obtain the output-variable's Cumulative Distribution Function (CDF), confidence interval and the Sobol indices of each input variable. Together, these quantities are used to suggest suitable ways of achieving accurate and repeatable predictions of propeller performance at intermediate Reynolds numbers.

2 Methods

In a sampling-based variance decomposition, a function, which is assumed to be a black box, is evaluated typically a large times and, based on its input values and its response through the output value, variance can be obtained, allowing to estimate the parameter uncertainty. However, one of the main drawbacks of this approach is that the quality of parameter uncertainty values is related on how many samples N_i of function f are evaluated on. This approach might become infeasible with CFD, depending on the case studied.

An alternative approach proposed in this work is to use an approximate function $\tilde{f}$ as a surrogate model, which has a considerably lower computational cost, as schematically represented in Fig. 1. In this approach, some points N need to be sampled from CFD solution and used to construct the surrogate model. This yields a response surface approximation $\tilde{f}$ which may be used for sampling thousands of N_i points.

Subsequently $\tilde{f}$ is obtained, it is possible to perform the Uncertainty Quantification. Given the input uncertainties $\mathbf{x}$, each with its Probability Density Function (PDF), the sampler uses the surrogate model $\tilde{f}$ to obtain the output uncertainties and Sobol indices (explained in the next section).

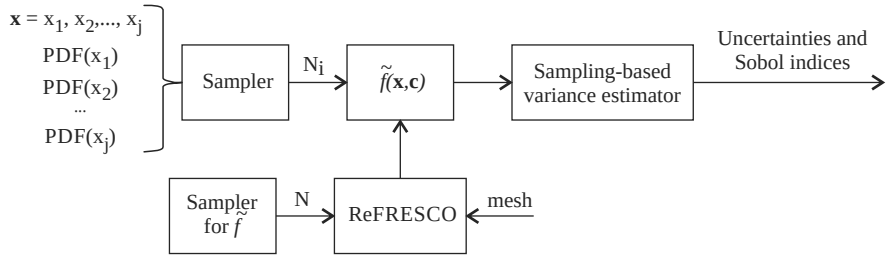

Fig. 1: Algorithm proposed in this work to perform Uncertainty Quantification in a sampling-based approach with CFD.

3 Sobol indices

Sobol indices of an output variable y_m associated with an input variable i denote the variance of the output, assuming the variable i is known (i.e., without uncertainty), divided by the variance of the output y_m, as expressed in Eq. (1). Therefore, a larger value of S_i means that the uncertainty in the input variable i has a larger effect on the variance of the output. Higher-order interaction index S_{i+j} has a similar meaning: variance decomposition by the interaction of the inputs i and j divided by the variance of the output. The sum of all Sobol indices, including the high-order terms, is equals to one. The total-order Sobol index ST_i is the sum of all Sobol indices which contains the input variable i, Eq. (1).

$$S_i = \frac{V_{x_i}\left(E_{\mathbf{x}\setminus x_i}\left(y_m|x_i\right)\right)}{V\left(y_m\right)} \qquad ST_i = \sum_{i\subset k} S_k \tag{1}$$

More detail about Sobol indices and their estimation are given by Saltelli et al. (2010).

4 Surrogate model

The basic idea behind an estimator is to sample a number of points through CFD simulations, feed the results to a regression model, thereby correlating the input and output values. The sampled points are chosen based on a Latin Hypercube Sampling (LHS). The mathematical operation used to create the surface response is linear interpolation between three nearest points when it is possible to create a concave surface. Extrapolation of order zero is used in other regions. This is done to avoid overshooting of results and ensure that the value is bounded within the range of simulated values. Figure 2 shows an example function estimator that considers a case with two inputs, shown on the x and y axes, and one output, plotted on the $z = Cf$ axis.

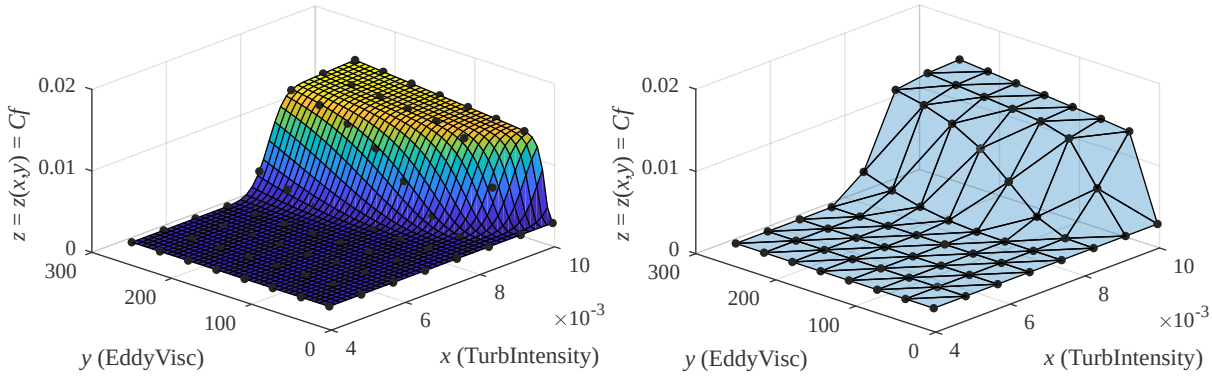

Fig. 2: Schema of function estimator: true response and sampled points (marked as black dots) from CFD results (left) and the surrogate model based on linear interpolation (right).

One drawback of using few points is the excessive use of extrapolation. To avoid it, sampling points are added on the edge of input variable range, yielding a so-called Shell Distribution sampling approach. Figure 3 shows an example of the use of Shell Distribution, LHS distribution and the combined distribution, assuming two inputs x_1 and x_2 characterised by triangular distributions bounded in [0; 1]. Shell Distribution also includes a point with the expected value of input variables, which may be interpreted as the mean input to the CFD simulation.

5 Duisburg Propeller Test Case - DPTC

This study is carried out with the propeller of the Duisburg Propeller Test-Case (DPTC) model P1570 of Ship Model Basin Potsdam (SVA). Pictures of DPTC and its CAD representation are shown in Fig. 4. Numerical and experimental studies with DPTC are presented in details in Wielgosz et al. (2019).

The chosen operating condition is close to the maximum efficiency point, $J = 0.8$, resulting in Reynolds number based on diameter of $Re_D = 2.43 \times 10^5$.

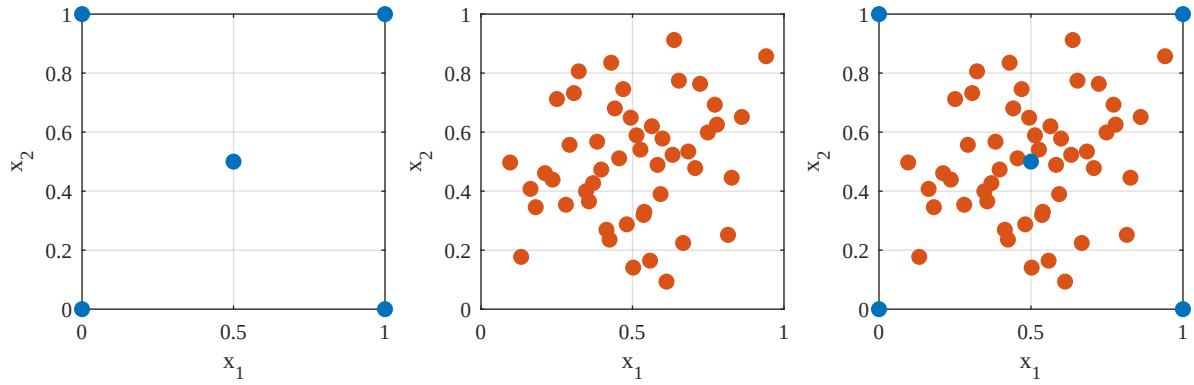

Fig. 3: Shell distribution (left); LHS distribution (center); and combined LHS+Shell distribution (right)

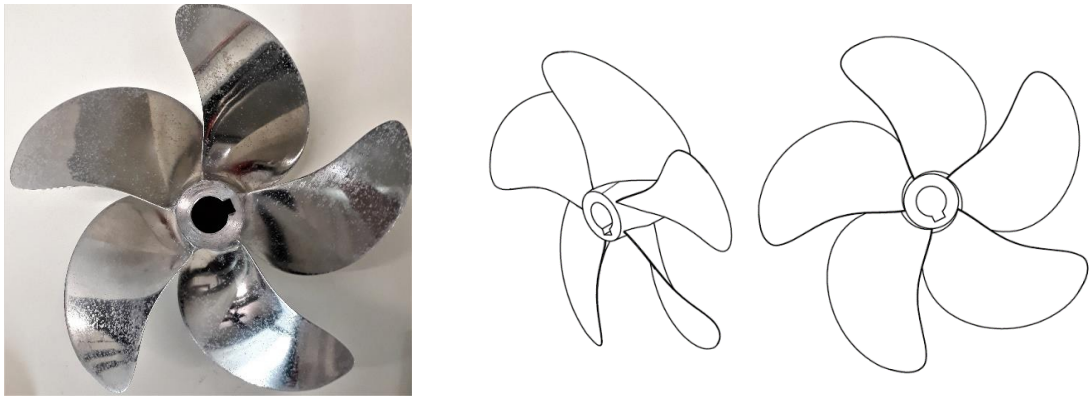

Fig. 4: Duisburg Propeller Test Case P1570. Figures extracted from Wielgosz et al. (2019)

6 Mesh topology

Two regions are used: a cylinder, which contains the rotating propeller, and a cylindrical grid, which represent the stationary part of the cavitation tunnel. The stator mesh is kept the same in all simulations and includes 1.1 million cells. For rotor region, five topologically identical grids with varying refinement levels were used. These varied between 5.2 and 31.2 million cells. Fig. 5 shows the five meshes and the gradation of element size on the blade surface.

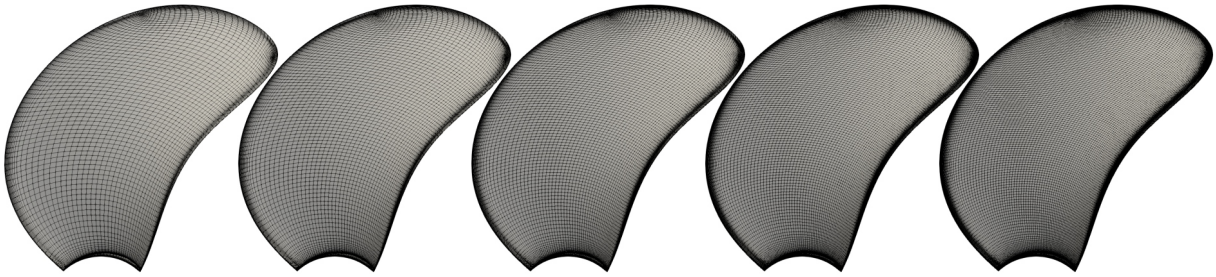

Fig. 5: Mesh elements on the blade.

7 Numerical Setup

Simulations are conducted using ReFRESCO (www.refresco.org), a community-based open-usage/open-source CFD code designed for marine applications, Vaz et al. (2009). Governing equations are discretised using a finite-volume approach and pressure-velocity coupling is solved using the SIMPLE algorithm. For momentum transport equations, `LIMITED QUICK` is used for the convective fluxes. $k-\omega$ SST 2003 turbulence model (Menter et al. (2003)) is used in conjunction with the $\gamma - \tilde{R}e_{\theta_t}$ transition model (Langtry and Menter (2009)). This model was Verified and Validated in Eça et al. (2016). Convective

fluxes of the turbulence equations are discretised with 1^{st} order upwind scheme. All diffusive fluxes are 2^{nd} order and the calculations are steady and in the Absolute-reference Frame Model (AFM).

8 Input Uncertainties and Analysed Outputs

Uncertainties of three input variables are considered: `powerTurbIntensity`, `powerEddyVisc` and `pDpx2FreezeTurb`.

Variable `powerTurbIntensity` is related exponentially to turbulence intensity at the inlet, Tu = 10^`powerTurbIntensity`. The PDF of this variable is assumed to be a uniform distribution. The lower bound is -3.301, which corresponds of $Tu = 0.0005$, smaller than the Selig's wind tunnel, which reportedly has a mean $Tu = 0.0007$ for highest Reynolds number test (Williamson et al. (2012)). The upper bound is -1.0, which corresponds of $Tu = 0.1$, chosen based on the mean value of Tu in rivers (McQuivey (1973)). Although the variable is uniformly distributed, the effect on Tu is exponential, which resembles a log-uniform distribution.

Variable `powerEddyVisc` is related exponentially to eddy viscosity ratio at the inlet, μ_t/μ = 10^`powerEddyVisc`. The PDF of this variable is assumed to be a uniform distribution. The lower bound is -1.301, which corresponds to $\mu_t/\mu = 0.05$. This value is chosen because it is half of lowest value used in Eça et al. (2016). The upper bound is 3.0, corresponding to $\mu_t/\mu = 1000$, twice of highest value used in Baltazar et al. (2018).

Variable `pDpx2freezeTurb` is not a boundary condition, but a parameter to artificially freeze the transport equation of turbulent kinetic energy, expressed in terms of a fraction of the propeller diameter. The PDF of this variable is assumed to be a uniform distribution, varying from 0.0 to 1.0.

It should be noted that the chosen input ranges can be considered conservative, since they are larger than values expected in most realistic scenarios, as well as extreme values reported in the literature. Therefore, it is expected that the computed parameter uncertainty will be considerable.

The analysed outputs correspond to typical open-water performance indicators, namely thrust coefficient K_T, torque coefficient K_Q, torque coefficient due to shear forces only $K_{Q,\,s}$ and hydrodynamic efficiency η_0. These are expressed as:

$$K_T = \frac{T}{\rho n^2 D_p^4}, \qquad K_Q = \frac{Q}{\rho n^2 D_p^5}, \qquad K_{Q,\,s} = \frac{Q_s}{\rho n^2 D_p^5}, \qquad \eta_0 = \frac{J}{2\pi}\frac{K_T}{K_Q}, \tag{2}$$

in which n is the rotation rate, D_p the propeller diameter, and $J = v_a/(nD_p)$ is the advance ratio based on free-stream velocity, v_a.

9 Results: Effect of CFD Sampling

To verify if the number of samples is sufficient to represent the surrogate model, three levels of sampling density are compared. All of them include a number of LHS samples plus 9 samples from the Shell distribution. This sensitivity study was carried out on the medium density grid. Figure 6 shows the CDFs of various responses for three sample sizes. The output values are divided by the mean value of output, showing the x axis in terms of percentage deviation from the mean value.

There is little variation in the CDFs of responses when increasing the number of samples from 29 to 49, indicating that 49 samples are sufficient to correctly represent the function estimator. Furthermore, because the studied input uncertainties were chosen to primarily affect the transition model behaviour, it was expected that the transition location, and consequently the viscous components of the predicted forces and moments, would see the largest response. Presented results indicate that among the analysed outputs, thrust coefficient experiences the smallest variation due to input uncertainties. Since this quantity is mainly influenced by the pressure distribution around the blade and not the shear forces, this trend is consistent with the aforementioned expectations. On the other hand, the shear stress distribution has a higher contribution to the torque than to the thrust and has been predicted to be the most affected by the variation of the inlet conditions, as evident form its largest uncertainty.

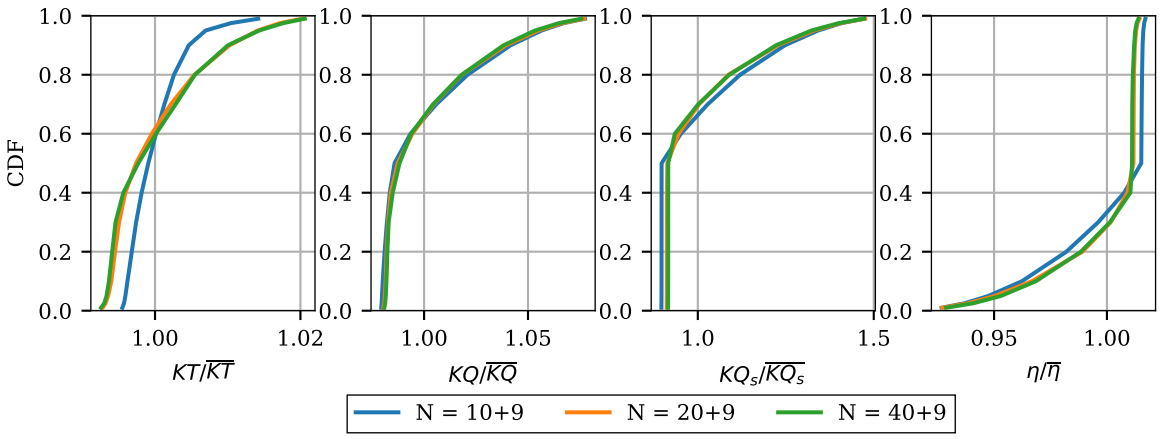

Fig. 6: Cumulative Density Function (CDF) of each output divided by the output expected value $E[Y]$ as a function of the number of elements N used to construct the respective surrogate models.

10 Results: Grid sensitivity study

Input uncertainty analysis was carried out for grids of varying densities, described in Sec. 6, using 49 sampling points. Key results of the analysis are the 95% confidence intervals of the outputs, as well as the associated Sobol indices. These are depicted in Figures 7 and 8 for the thrust and torque coefficients, respectively. For the latter, only the shear force contribution is considered. Left parts of the figures show bars in which the bottom and top represent the bounds of the 95% confidence interval coloured proportionally to each Sobol index. On the right-hand side of the figures, Total-order Sobol indices are shown on an absolute scale, alongside the individual values shown using colour bars. At each mesh refinement h/h(finest) the vertical bars are offset slightly for readability, knowing that where one Sobol contribution ends the next one starts. Subscripts 1, 2 and 3 refer to input variables `powerTurbIntensity`, `powerEddyVisc`, and `pDpx2FreezeTurb`, respectively.

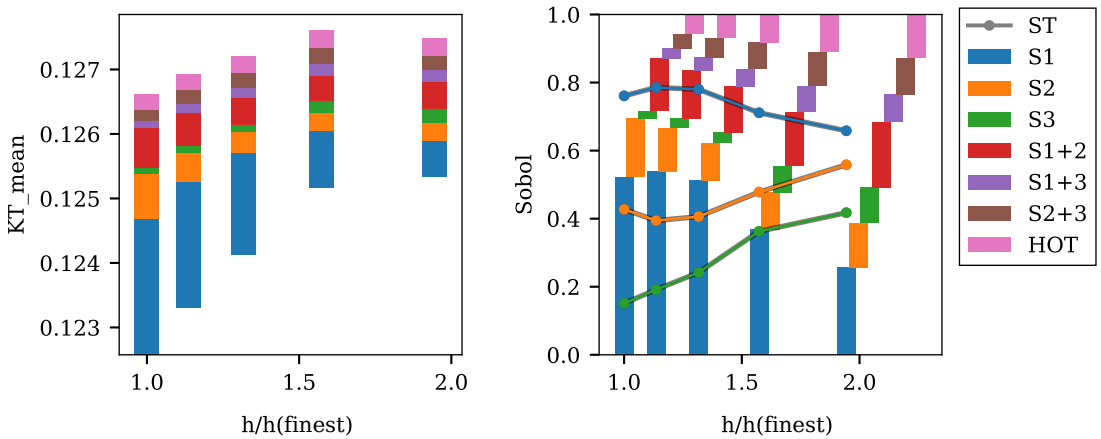

Fig. 7: Thrust Coefficient KT - 95% Confidence Interval (left) and Sobol Indices with the Total-Sobol contribution (right) for each mesh refinement. HOT indicates S1+2+3.

The results show that the confidence intervals change considerably with the mesh density for the K_T output but remains almost constant for the shear component of the torque coefficient $K_{Q,\,s}$ case. As discussed before, K_T is less affected by the parameter uncertainty, so the result may be explained by a higher influence of the discretisation uncertainty. On the other hand, $K_{Q,\,s}$ is more sensitive to parameter uncertainty, making the relative effect of the discretisation uncertainty less pronounced.

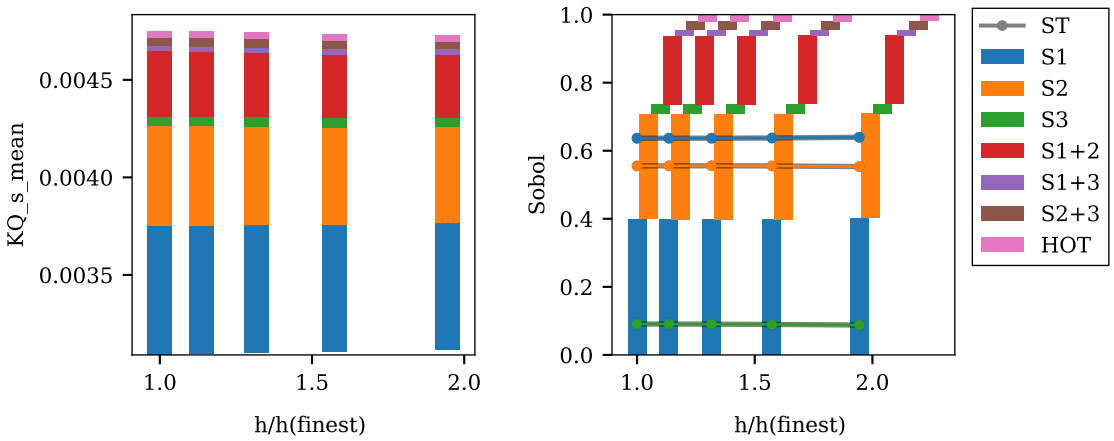

Fig. 8: Torque Coefficient of Shear Stress contribution only KQ_s - 95% Confidence Interval (left) and Sobol Indices with the Total-Sobol contribution (right) for each mesh refinement. HOT indicates S1+2+3.

11 Conclusions

Using a surrogate model instead of direct sampling through CFD runs has been shown to be an effective approach for performing uncertainty quantification analysis of CFD simulations.

The results also showed that, depending on the analysed output, there is a considerable co-dependence between parametric and discretisation uncertainties. In the future, it is considered important to couple the uncertainty of the inputs and the grid refinement studies to obtain a combined uncertainty, taking into account the combined effect of both sets of parameters and their covariance.

The input variables chosen for this test case were focused mainly to understand the transition effect due to uncertainties on the boundary conditions. The proposed model can be used for other similar applications, including other input uncertainties. For example, based on experimental uncertainties to determine the advance velocity or rotation rate on a cavitation tunnel, the presented method can be used to estimate the impact of these uncertainties on the main indicators of open-water propeller performance.

References

J. Baltazar, D. Rijpkema, J. Falcão de Campos (2018). On the use of the Gamma-ReTheta transition model for the prediction of the propeller performance at model-scale. *Ocean Engineering*, **170**(August), 6-19.

L. Eça, R. Lopes, G. Vaz, J. Baltazar and D. R. Rijpkema (2016). Validation Exercises of Mathematical Models for the Prediction of Transitional Flows. Proceedings of 31st Symposium on Naval Hydrodynamics, Monterey, Canada.

R. B. Langtry and F. R. Menter (2009). Correlation-based transition modeling for unstructured parallelized computational fluid dynamics codes. *AIAA Journal*, **47**(12), 2894-2906.

R. Lopes, L. Eça, G. Vaz (2018). Assessment of RANS Transition Models. Proceedings of 21st NuTTS, Italy

R. S. McQuivey (1973). Summary of Turbulence Data from Rivers, Conveyance Channels, and Laboratory Flumes: Turbulence in Water. US Government Printing Office.

F. R. Menter, M. Kuntz and R. Langtry (2003). Ten Years of Industrial Experience with the SST Turbulence Model Turbulence heat and mass transfer. *Turbulence, Heat and Mass Transfer*, **4**, 625-632.

F. R. Menter, R. B. Langtry, S. R. Likki, Y. B. Suzen, P. G. Huang and S. Vo'Ilker, S. (2004). A Correlation-Based Transition Model Using Local Variables: Part I - Model Formulation. *ASME Turbo Expo*, **128**, 57-67.

A. Saltelli, P. Annoni, I. Azzini, F. Campolongo, M. Ratto, and S. Tarantola (2010). Variance based sensitivity analysis of model output. Design and estimator for the total sensitivity index. *Computer Physics Communications*, **181**(2), 259-270.

G. Vaz, F. Jaouen, and M. Hoekstra (2009). Free-Surface Viscous Flow Computations: Validation of URANS Code. Polar and Arctic Sciences and Technology; CFD and VIV, pages 425-437.

C. Wielgosz, R. Golf, A. K. Lidtke, G. Vaz and O. Moctar (2019). Numerical and experimental study on the Duisburg Propeller Test Case. Proceedings of 22nd NuTTS, Tomar, Portugal.

G. A. Williamson, B. D. McGranahan, B. A. Broughton, R. W. Deters, J. B. Brandt and M. S. Selig (2012). Summary of Low-Speed Airfoil Data : Volume 5. PhD thesis, University of Illinois at Urbana-Champaign.